ACS Sustainable Chemistry & Engineering

Research Article

Cite This: ACS Sustainable Chem. Eng. 2019, 7, 6813−6820

pubs.acs.org/journal/ascecg

Photocatalytic Fixation of Nitrogen to Ammonia by Single Ru Atom Decorated TiO_2 Nanosheets

Shizhen Liu,[†] Yajun Wang,[‡] Shaobin Wang,[§] Mingmu You,[‡] Song Hong,[†] Tai-Sing Wu,[⊥] Yun-Liang Soo,[⊥] Zhenqing Zhao,[†] Guiyuan Jiang,*[,‡] Jieshan Qiu,[†] Baojun Wang,*[,∥] and Zhenyu Sun*[,†]

[†]State Key Laboratory of Organic−Inorganic Composites, College of Chemical Engineering, Beijing University of Chemical Technology, Beijing 100029, P. R. China

[‡]State Key Laboratory of Heavy Oil Processing, China University of Petroleum (Beijing), Beijing 102249, P. R. China

[§]School of Chemical Engineering, The University of Adelaide, Adelaide SA 5005, Australia

[∥]Key Laboratory of Coal Science and Technology of Ministry of Education and Shanxi Province, Taiyuan University of Technology, Taiyuan 030024, P. R. China

[⊥]Department of Physics, National Tsing Hua University, Hsinchu 30013, Taiwan

Supporting Information

ABSTRACT: Photocatalysis shows a great potential for N_2 fixation to NH_3 under mild conditions, which intrigues increasing research attention in recent decades. To this end, the design of efficient photocatalysts is the key. Herein, we report the synthesis of single atom Ru decorated TiO_2 nanosheets rich in oxygen vacancies. Single Ru sites greatly promoted photoreduction of aqueous N_2 to NH_3, affording an NH_3 formation rate of 56.3 $\mu g/h/g_{cat}$. We found that isolated Ru atoms likely weakened the hydrogen evolution, promoted absorption of N_2, and also improved the charge carrier separation, which led to enhanced N_2 photofixation.

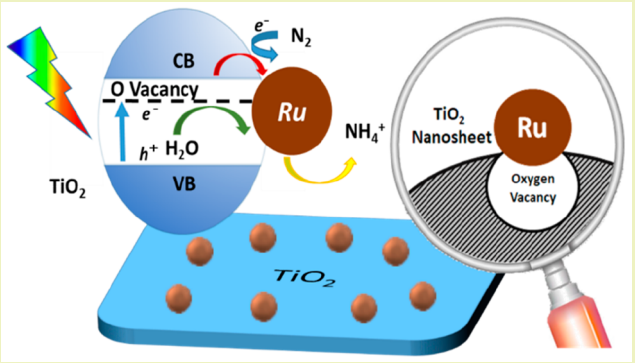

KEYWORDS: *N_2 fixation, Ammonia, Photocatalysis, Single atom, TiO_2, Ru*

INTRODUCTION

Ammonia has been greatly demanded in civilization development. However, the conventional Haber−Bosch process for ammonia production requires drastic reaction conditions (15−25 MPa, 300−550 °C), leading to high energy wasting and environmental issues.[1,2] Photocatalysis has been considered as an environmentally friendly procedure with sunlight illumination as an energy source, and holds promise for N_2 fixation at mild conditions by using dissolved nitrogen with water.[3,4] In recent decades, photocatalysts such as TiO_2,[5] MoS_2,[6,7] g-C_3N_4,[8−10] black phosphorus,[11] BiOBr,[12] and ZnO[13] have shown photocatalytic activities for N_2 reduction.

TiO_2 is a typical d^0 semiconductor[14] with a suitable conduction band (CB) (E_{CB} = −0.29 V vs SHE) to drive N_2 reduction to NH_3.[15−20] However, most of the photocatalysts in N_2 fixation applications suffer from drawbacks such as (1) high adsorption energy of N_2 on catalyst surface; (2) poor activity under visible light; and (3) insufficient charge carriers on the catalyst surface due to swift recombination.[21,22] Thus, modifications are essential to improve a photocatalyst's performance for efficient N_2 reduction. Transition metal doping is beneficial to photocatalysis.[23,24] Recently, Zhao and co-workers modified TiO_2 by Fe^{3+} with highly exposed (101) facets to show high efficiency for N_2 photofixation.[25] Fe^{3+} with a radii of 0.64 Å was able to replace Ti^{4+} (radii of 0.68 Å) in the lattice, which enabled the generation of oxygen vacancy (V_o) for active radical production. Meanwhile, Ti^{3+} ion led to stronger adsorption of N_2 and cleavage of the N≡N bond.[23,26] In addition, noble metals have been attempted to enhance N_2 photofixation on TiO_2.[23] Compared to Fe, ruthenium (Ru) exhibits a significantly lower N_2 reduction overpotential, thus holding potential in modifying TiO_2 for improved photocatalytic N_2 fixation.[27−29]

The size of catalysts directly influences the number of low-coordinated surface sites, which has profound impacts on the reactant binding strength and governs the catalytic performances to a great degree. Recently, single atom-based catalysts have attracted intensive attention due to their outstanding catalytic activities in many reactions.[30,31] Notably, single atom metals dispersed on supports feature homogeneity of catalyti-

Received: November 24, 2018
Revised: February 7, 2019
Published: February 27, 2019

DOI: 10.1021/acssuschemeng.8b06134
ACS Sustainable Chem. Eng. 2019, 7, 6813−6820

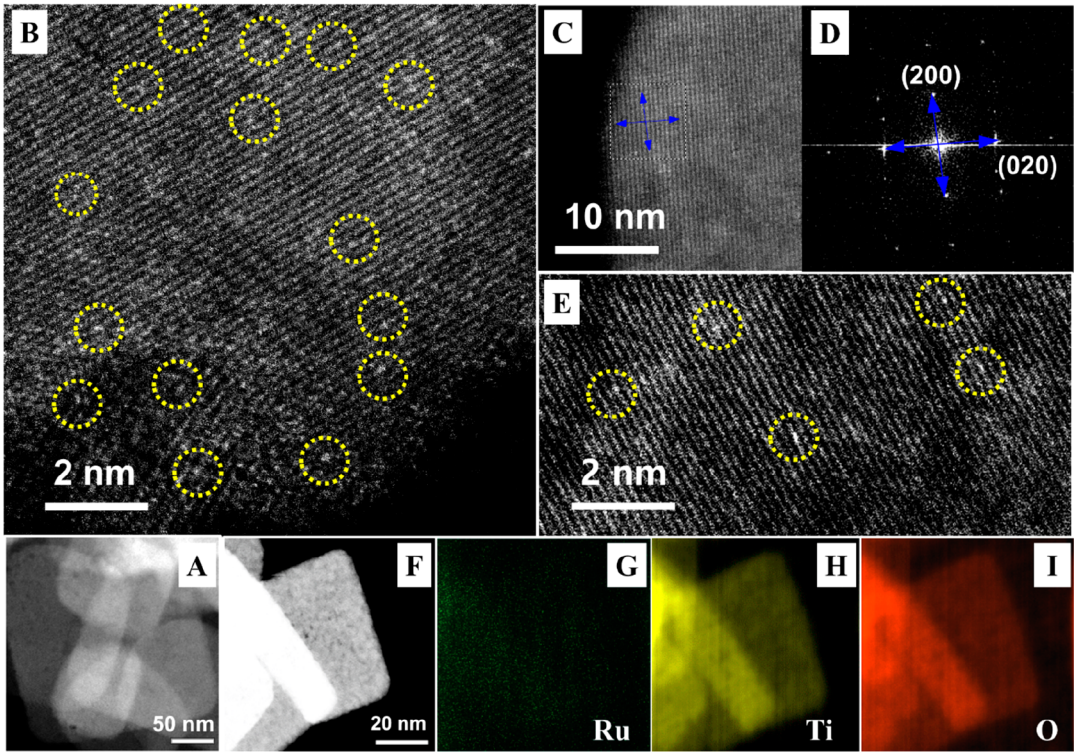

Figure 1. (A) SEM, and (B, C) HAADF-STEM images of TR-1.0. (D) FFT analysis of the area shown in (C). (E, F) HAADF-STEM images of Ru single atom decorated TiO_2 nanosheets. EDX mapping images of Ru (G), Ti (H), and O (I) elements over the region shown in (F).

cally active sites, low-coordination environment of metal atoms, and maximum metal utilization efficiency. These characters endow single atom catalysts with remarkable catalytic activity, stability, and selectivity for a range of processes.[32−34] Nonetheless, single atom photocatalysis in NH_3 synthesis has been seldom reported to date.

Herein, we demonstrate single atom Ru decorated TiO_2 nanosheets with engineered oxygen vacancy for photocatalytic N_2 fixation. The existence of single Ru sites has been investigated by X-ray absorption near edge structure (XANES) spectroscopy and high-angle annular dark-field scanning transmission electron microscopy (HAADF-STEM). The loading of 1 wt % Ru on TiO_2 nanosheets enabled significant enhancement in photocatalytic N_2 reduction. Ru addition was able to not only adsorb N_2 molecules but also enhance charge separation.

RESULTS AND DISCUSSION

The X-ray diffraction (XRD) patterns of as-prepared samples are given in Figure S1. Characteristic reflection peaks of anatase TiO_2 (JCPDS no. 21-1272) can be seen in all the cases; however, no reflections of Ru are observed probably due to its amorphous structure and/or low loading, which rules out the formation of large Ru aggregates.[35] A number of nanosheets are overlapped each other for TiO_2-NS (Figures 1A and S2A). Aberration-corrected high-angle annular dark field scanning transmission electron microscopy (HAADF-STEM) observation (Figures 1B,E,F, and S2B) and in situ EDX (Figure S2D) together with elemental mapping (Figure 1G−I) show the presence of bright spots, which can be ascribed to Ru atoms because Ru has a higher atomic number than Ti and O. The lateral sizes of TiO_2 nanosheets before and after decoration of Ru were similar, which were estimated to be about 40 nm by TEM (Figure S2B,C). The (200) and (020) facets of TiO_2-NS have been observed, as shown in the high-resolution STEM image (Figure 1C) along with fast Fourier transform (FFT) (Figure 1D), reflecting the exposed (001) plane.[36] Some Ru atoms are annotated with yellow dashed circles (Figure 1B,D,E). In stark contrast, for pristine TiO_2 without oxygen vacancies (TR-ND), Ru is present predominantly in clusters and small nanoparticles, as revealed in Figure S3A,B. Likewise, at a higher Ru loading (2 wt %), relatively larger Ru nanoparticles of up to 5 nm are observed (Figure S3C).

The surface composition and chemical state of the TR-1.0 sample were studied by X-ray photoelectron spectroscopy (XPS). The Ti 2p core-level XPS spectra of the TR-1.0 sample consist of Ti $2p_{3/2}$ and Ti $2p_{1/2}$ peaks (Figure 2A) with binding energies (BEs) at 458.4 and 464.4 eV, which are assigned to the Ti^{4+}. A deconvoluted peak appearing at 463.3 eV may result from the $3p_{3/2}$ orbital electron of Ru and can be assigned to Ru^{3+}.[37] In the O 1s XPS spectra of TR-1.0 (Figure 2B), besides the peak at 529.7 eV corresponding to the Ti-O-Ti, a weak peak with BE at 531.2 eV was also observed arising from oxygen vacancies introduced due to thermal H_2 treatment.[38] In the Ru $3p_{3/2}$ XPS spectra, the peak at about 531.6 eV likely originated from RuO_x due to oxidation of Ru after exposure to air.[39] An additional peak centering at 533 eV was also identified, possibly assigned to surface H_2O (adsorbed oxygen) because of the strong hydrophilicity of oxygen vacancies.[40] Moreover, density functional theory (DFT) calculations were performed to explain the stability of Ru atoms on the surface TiO_2 nanosheets. All results are based on perfect and defective TiO_2(001) surface structures. Oxygen vacancies of D-O-2v and D-O-3v could be generated from two-fold coordinated O-2c and three-fold coordinated O-3c respectively, as shown in the upper panel of Figure 2C). The adsorption energy of Ru (E_{ads})

DOI: 10.1021/acssuschemeng.8b06134
ACS Sustainable Chem. Eng. 2019, 7, 6813−6820

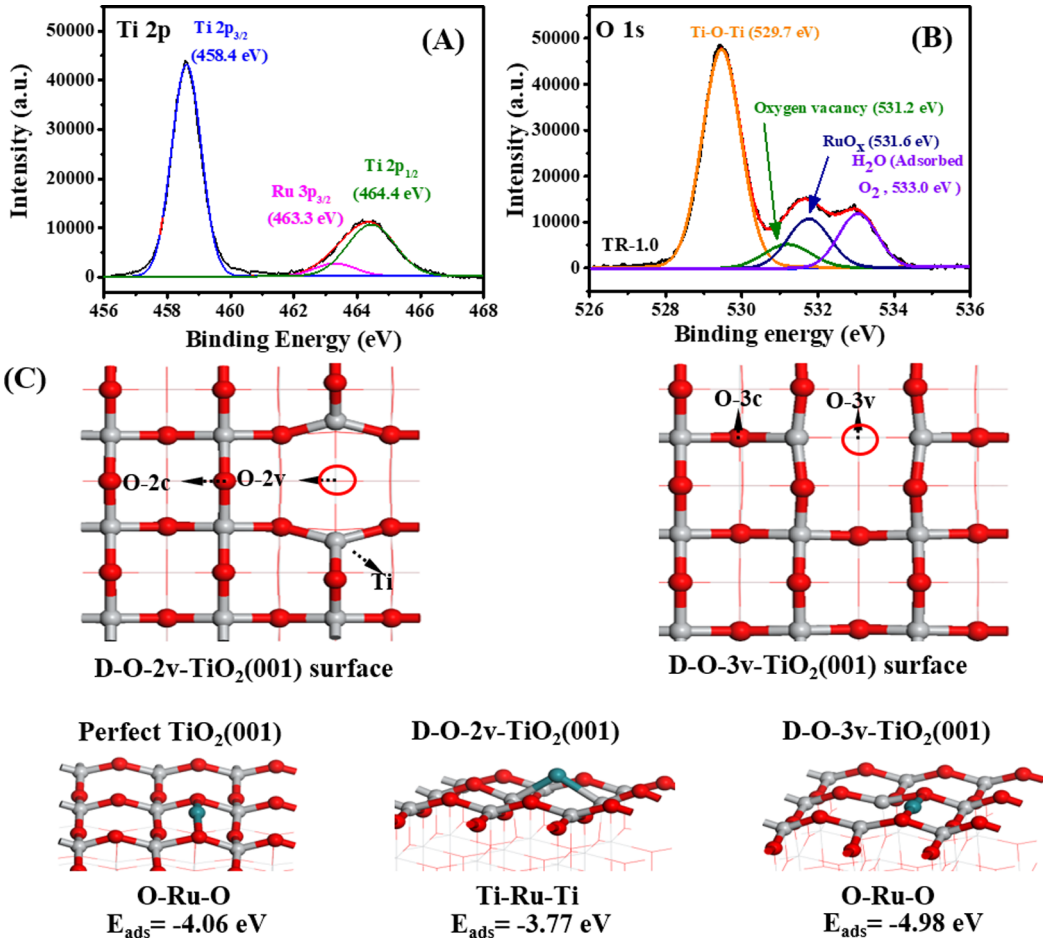

Figure 2. (A) Ti 2p and (B) O 1s XPS spectra of TR-1.0 catalyst. (C) The optimized structure of the TiO_2(001) surface (upper layer) and the most stable binding states and their relative adsorption energies of Ru atomic sites supported on the perfect, O-2v, and O-3v defective surfaces (bottom layer).

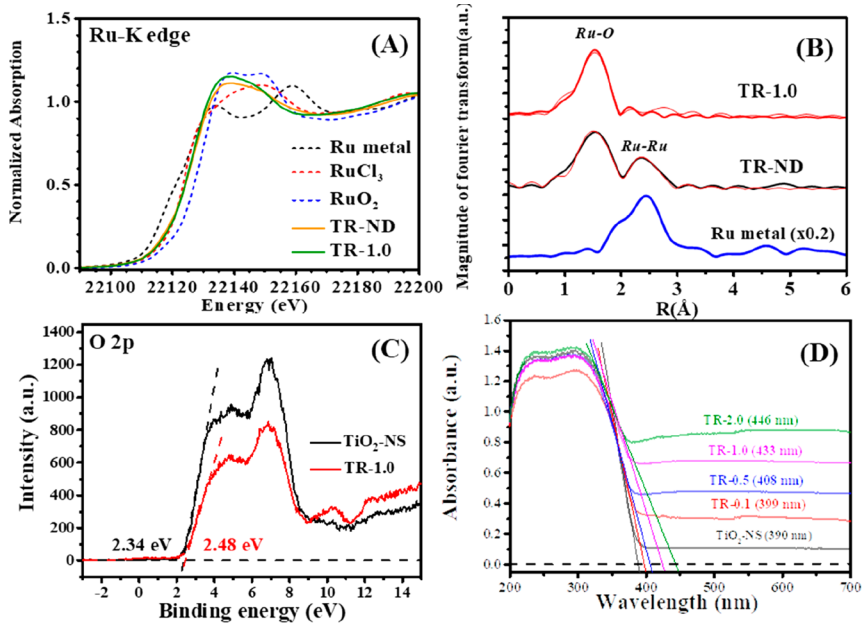

Figure 3. (A) XANES spectra of Ru K-edge on TR-ND and TR-1.0. (B) EXAFS spectra of Ru K-edge on TR-1.0, and Ru metal. (C) O 2p XPS VB spectra of pure TiO_2-NS and TR-1.0. (D) UV−vis absorption spectra of TiO_2-NS, TR-0.1, TR-0.5, TR-1.0, and TR-2.0.

on perfect TiO_2(001), D-O-2v-TiO_2(001), and D-O-3v-TiO_2(001) were calculated to be −4.06, −3.77, and −4.98 eV, respectively. The O-Ru-O structure over defective TiO_2 nanosheets had the highest adsorption energy, thus favoring

DOI: 10.1021/acssuschemeng.8b06134
ACS Sustainable Chem. Eng. 2019, 7, 6813−6820

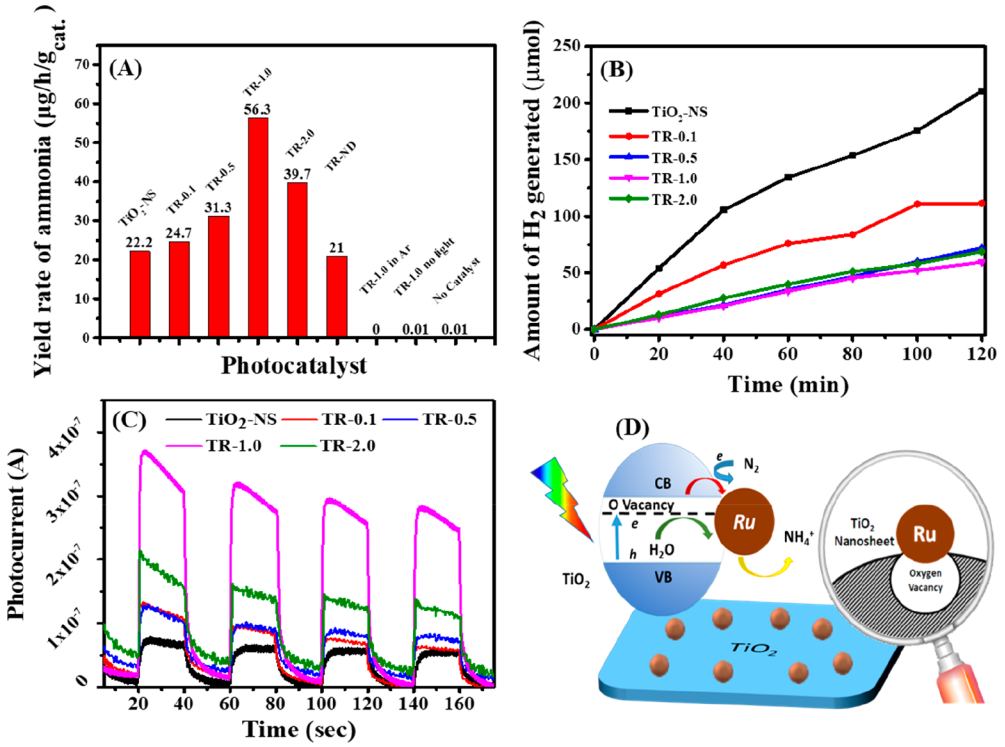

Figure 4. (A) The yield rates of ammonia over TiO_2-NS, TR-0.1, TR-0.5, TR-1.0, TR-2.0, and TR-ND. (B) The amounts of H_2 generated over TiO_2-NS, TR-0.1, TR-0.5, TR-1.0, and TR-2.0 in water. (C) Transient photocurrent responses of TiO_2-NS, TR-0.1, TR-0.5, TR-1.0, and TR-2.0. (D) Mechanistic diagram of N_2 photoreduction over single Ru site loaded TiO_2 nanosheets with oxygen vacancies.

formation and dispersion of single Ru atoms especially on oxygen vacancy sites. More theoretical calculation details can be found in Table S1. The projected d-band partial density of states (pDOS) results of Ru and O are illustrated in Figure S4. Compared with the electron densities of absorbed Ru_{4d} and O_{2p} over the perfect $TiO_2(001)$ surface, the electron densities of the D-O-3v-$TiO_2(001)$ surface shift to lower energies, leading to enhanced Ru−O interaction. Therefore, the Ru−O bond is more stable.

To verify the formation of Ru single atoms in TR-1.0, XANES measurements were performed. The XANES spectra (Figure 3A) show that the absorption threshold of Ru in TR-1.0 approaches that of $RuCl_3$, suggesting that the valence state of Ru is close to 3+. In the Ru K-edge EXAFS spectrum of TR-1.0, only a predominant peak at ca. 1.5 Å is observed and no scattering from metallic Ru−Ru is discernible (Figure 3B).[41] This supports the hypothesis that Ru in TR-1.0 is mainly atomically dispersed. Whereas a pronounced peak at ca. 2.3 Å is identified for TR-ND, corresponding to metallic Ru−Ru (Figure S5). This indicates that the aggregation of Ru would take place when there are no oxygen vacancies on TiO_2, consistent with TEM observation.[42]

Electron paramagnetic resonance (EPR) analysis was used to probe O vacancies in TR-*x* samples. The EPR peaks between 3440 and 3530 could result from an O vacancy.[5] As expected, TiO_2-ND does not show clear signals of O vacancy (Figure S6A). In contrast, an EPR peak associated with an O vacancy is observed for TR-NS (Figure S6B). The signal intensity of O vacancy for TR-1.0 (Figure S6C) drops in comparison to that of TR-NS, due to the occupation of Ru atoms in the O-vacancy sites.[5]

The O 2p XPS valence-band (VB) spectra were analyzed from −3 to 15 eV (Figure 3C). The TiO_2 sample exhibited an apparent peak of the O 2p orbital at 2.34 eV to build up valence in the catalyst. In contrast, the top of the VB of TR-1.0 was shifted to 2.48 eV probably arising from the increase in the upward band bending as a result of interaction between TiO_2 and Ru.[40,43,44] UV−vis spectroscopy revealed that the Ru loaded TiO_2 nanosheet photocatalysts exhibited a wider absorption range than pure TiO_2 nanosheets (Figure 3D). The absorption edges of TiO_2-NS, TR-0.1, TR-0.5, TR-1.0, and TR-2.0 were at 390, 399, 408, 433, and 446 nm, respectively. The corresponding band gap energies can be estimated to be 3.28, 3.21, 3.14, 2.96, and 2.87 eV. Accordingly, the CBs of the TiO_2-NS and TR-1.0 VBs can be derived to be −0.94 and −0.48 V (vs SHE), which are suitable to drive N_2 reduction to NH_3 ($N_2 + 6e^- + 6H^+ \rightarrow 2NH_3$, E^0_{redox} = 0.0944 V vs SHE).[17,18,45]

The photocatalytic activities of single atom Ru loaded TiO_2 nanosheets for N_2 fixation were tested in a N_2 bubbled water system using a 300 Xe lamp as a light source. The experiments were carried out continuously for 4 h, and the final NH_4^+ ion content was measured by the indophenol blue indicator method (Figure S7). Catalytic experiments in Ar-saturated solution, or without any catalyst, or in the dark without light irradiation have been also performed, which however showed very little NH_3 generation. The ammonia yield rates over TR-*x* catalysts are presented in Figure 4A. We found that the addition of single atom Ru is able to enhance the photocatalytic activities of TiO_2 nanosheets, evidenced by higher ammonia yield rates. The TR-1.0 catalyst delivers the highest ammonia yield rate of 56.3 $\mu g/h/g_{cat.}$ with good reproducibility (Figure S8), and reasonable stability (Figures S9 and S10), 2 times higher than TiO_2-NS. Compared with oxygen vacancy-deficient TiO_2-ND, the samples with oxygen vacancies show enhanced ammonia yield rates. This indicates that oxygen

DOI: 10.1021/acssuschemeng.8b06134
ACS Sustainable Chem. Eng. 2019, 7, 6813−6820

vacancy sites likely promote N_2 activation. Further research in tuning of oxygen vacancy concentration by manipulating conditions (including annealing atmosphere such as H_2, Ar, CO, or N_2 and temperature) for N_2 reduction will be systematically conducted in our future work.

We also investigated the photocatalytic properties of Ru decorated TiO_2 nanosheets for H_2 evolution reaction (HER), which usually occurs as a competitive reaction during the photocatalytic N_2 reduction process. The results (Figure 4B) show that the photocatalytic activities of TiO_2 nanosheets for HER decrease upon decoration with Ru. Pure TiO_2 nanosheets generated the largest amount of H_2 after light illumination for 2 h, providing a H_2 production rate of up to 105.3 μmol/h (per 10 mg photocatalyst). Whereas the HER becomes weakened with the increase of Ru content before reaching an almost saturated value of 30 μmol/h (per 10 mg photocatalyst) at the Ru content of 0.5 wt %. It has been proposed that the oxygen vacancies in TiO_2 nanosheets are the key active sites for HER.[46] In our case, we believe that Ru species likely replaced H_2O molecules to combine with the oxygen vacancies, which thus disturbed the transportation of photoelectrons from TiO_2 to H^+, inhibiting HER. Photocurrent transient response was used to explore the photogenerated charge carriers under irradiation (Figure 4C). The results showed that Ru loading can enhance the photocurrent of TiO_2-NS. This is especially the case for the TR-1.0 catalyst exhibiting the highest photocurrent intensity. TR-2.0 also displayed a high photocurrent despite being lower than that of the TR-1.0 sample because the aggregation of Ru at high loading weakened illumination absorption of TiO_2.[23]

On the basis of the above results, we propose a possible mechanistic understanding of N_2 photoreduction over Ru loaded TiO_2 nanosheets, as shown in Figure 4D. The calcination in a reducing atmosphere led to formation of oxygen vacancies on the surface of TiO_2 nanosheets,[47] as evidenced by XPS and EPR results.[47] This may promote photocatalytic HER over TiO_2 nanosheets. Despite this being the case, Ru atoms deposited on the oxygen vacancy sites of TiO_2 nanosheets could reduce H_2 evolution rate during the photocatalytic N_2 reduction (Figure 4D).

The upward band bending of atomic Ru loaded TiO_2 nanosheets can be revealed by electronic band structure analysis, as illustrated in Figure S11. On the perfect TiO_2(001) surface, the O-Ru-O band is symmetrical and shares the same electronic band structures of TiO_2. However, on the D-O-3v-TiO_2(001) surface, the O-Ru-O is no longer symmetrical owing to the dangling bonds around O vacancies, which leads to splitting of the Ti 3d states. Hence the D-O-3v-TiO_2(001) exhibits a narrowed band gap because of the generated intermediate level. The electron transition energy from VB to CB minimum is 0.227 eV, in contrast to the value of 0.435 eV on perfect TiO_2(001). Furthermore, the empty d orbitals of Ru may accept photoelectrons to reduce the recombination of photocarriers. According to the Nyquist plots (Figure S12) derived from electrochemical impedance spectroscopy, TR-1.0 shows a smaller arc and facilitates more effective charge separation and faster charge transfer than pristine TiO_2 nanosheets, thereby benefiting photocatalysis.[48,49] Furthermore, Ru possesses a small activation barrier for N_2 dissociation.[50] As a consequence, we speculate that Ru is likely the center for N_2 adsorption[26] and activation with single atoms being more active than clusters or nanoparticles.[30,51,52] However, the overloading of Ru led to the decrease of photocatalytic activity for ammonia generation probably due to the aggregation of Ru.

CONCLUSIONS

We have designed and fabricated TiO_2 nanosheets decorated with Ru atoms, which enabled photocatalytic reduction of N_2 to ammonia under xenon lamp illumination. DFT calculations indicated that single Ru sites are stabilized by O vacancies. The composite catalyst containing 1 wt % of Ru showed a significantly improved ammonia generation rate of up to 56.3 $\mu g/h/g_{cat.}$, more than 2 times higher than pure TiO_2 nanosheets. Isolated Ru atoms that were possibly located at the oxygen vacancies of TiO_2 helped weaken the hydrogen evolution, promote chemisorption of N_2, and also improve charge carrier separation, leading to enhanced N_2 photoreduction to ammonia. We believe that the development of single atom catalysts provides a potentially alternative avenue for efficient N_2 photofixation.

EXPERIMENTAL SECTION

Materials. Tetra-*n*-butyl titanate ($Ti(OBu)_4$, TBOT, 99.0%), sodium hydroxide (99.9%), ethanol (99.8%), hydrofluoric acid solution (HF, 40 wt %), and ruthenium chloride hydrate were obtained from Aladdin. All the chemicals used in this work were of analytical grade without pretreatment.

Synthesis of TiO_2 Nanosheets. In a typical procedure for TiO_2 nanosheet synthesis, 13 mL of hydrofluoric acid solution (40 wt %) was dropped into 25 mL of TBOT under vigorous stirring for 2 h. Then the mixture was transferred into a 50 mL Teflon-lined autoclave and hydrothermally treated at 180 °C for 36 h. After cooling down to room temperature, the suspension was isolated by a high-speed centrifuge and washed with ethanol and distilled water for several times. Then the precipitate was dispersed in 0.1 M NaOH solution for 8 h at room temperature under stirring to remove residue F ions. The obtained powder was recovered by centrifugation, followed by washing with distilled water and drying at room temperature to obtain TiO_2 nanosheets. The above dried powder was thermally treated in a hydrogen−argon mixture (8.0 vol % hydrogen) at 250 °C for 2 h. This treatment is supposed to introduce oxygen vacancies on the surface of TiO_2 nanosheets, beneficial to further deposition of Ru. The resulting TiO_2 nanosheets were referred to as TiO_2-NS.

Preparation of Ru-TiO_2 Nanosheets. The obtained TiO_2 nanosheets (200 mg) were ultrasonically dispersed in 20 mL of ethanol for 1 h. Then, 0.15 mL of ruthenium chloride hydrate-ethanol solution (4.4 mg/mL) was added dropwise into the suspension under stirring. Afterward, the mixture was stirred for 6 h. The precipitate was filtered, washed with water, and vacuum-dried at 60 °C to obtain a Ru-TiO_2 NS, which was further thermally treated in a tube furnace in a hydrogen−argon atmosphere (8.0 vol % hydrogen) at 250 °C for 2 h. The generated powder was referred to as TR-0.1. For preparation of other TR-0.5, TR-1.0, TR-2.0 samples, similar procedures were adopted except that the amounts of the ruthenium chloride hydrate-ethanol solution were 0.75, 1.5, and 3.0 mL, respectively. A TR-ND sample was prepared by following a similar process except that the calcination was carried out in air.

Characterization. X-ray powder diffraction (XRD) was performed on a D/MAX−RC diffractometer operated at 30 kV and 100 mA with Cu Kα radiation and a 2θ scan rate of 5°/min. Transmission electron microscopy (TEM) images were obtained by a JEOL ARM200 microscope. TEM samples were prepared by depositing a droplet of a suspension onto a lacey carbon film. X-ray photoelectron spectroscopy (XPS) experiments were carried out by a Thermo Scientific ESCALAB 250Xi instrument equipped with an electron flood and scanning ion gun. The XPS spectra were calibrated by C 1s binding energy at 284.8 eV. UV−vis diffuse reflectance spectra (DRS) were obtained using Persee UV−vis spectroscopy (TU-1950, $BaSO_4$ as a reference). The XAFS measurements were performed in a

DOI: 10.1021/acssuschemeng.8b06134
ACS Sustainable Chem. Eng. 2019, 7, 6813−6820

fluorescence mode using a Lytel detector at beamline BL07A of Taiwan Light Source, NSRRC. A Si(111) Double Crystal Monochromator (DCM) was used to scan the photon energy. The energy resolution ($\Delta E/E$) for the incident X-ray photons was estimated to be 2×10^{-4}. Quantitative information on the radial distribution of neighboring atoms surrounding Ru was derived from the extended absorption fine structure (EXAFS) data. An established data reduction method was used to extract the EXAFS χ-functions from the raw experimental data using the IFEFFIT software. To ascertain the reproducibility of the experimental data, at least two scans were collected and compared for each sample. EPR spectra were obtained using a Bruker e-scan EPR spectrometer (27 °C, 9.7397 GHz).

Photocatalytic N_2 Fixation. Photocatalytic N_2 fixation was carried out in a N_2 gas reactor under artificial illumination at room temperature and atmospheric pressure. In the first step, 40 mg of a photocatalyst was added in a 100 mL of 20% ethanol solution in a quartz reactor. Then the system was thoroughly sealed and linked with a 20 mL 0.1 mol/L HCl gas-washing bottle to recover the NH_3 gas from reacted tail gas. Afterward, N_2 gas was introduced into the reactor and bubbled in the solution for 1 h to remove air from the system under 350 rpm stirring. N_2 bubbling was maintained during the whole reaction process. Subsequently, the reactor was irradiated by a 300 W high pressure xenon lamp (PLS-SXE300, Beijing Perfect Light Technology Co., Ltd. China). The photoreaction temperature was kept at 25 °C using a thermostat bath. After 4 h of continuous irradiation, the reactor was unsealed and 5 mL of the solution was taken from the reactor by a syringe with a syringe filter (filter aperture 0.22 μm) to remove all particles. The transparent solution was used for detection of NH_3.

During the photocatalytic N_2 fixation reaction, the light resource was placed 0.11 m away from the reaction solution surface. The irradiation intensity between 280 and 400 nm was measured by a SENTRY 524 irradiance meter, giving the value of 34.87 mW/cm^2. The intensity of wavelength between 400 and 1000 nm irradiation was measured to be 1403 mW/cm^2 by an FZ-A irradiance meter.

■ ASSOCIATED CONTENT

Supporting Information

The Supporting Information is available free of charge on the ACS Publications website at DOI: 10.1021/acssuschemeng.8b06134.

Experimental and DFT calculation details; XRD patterns; TEM images with EDX spectrum; SEM images; XANES spectra; calculated pDOS; UV−vis absorption spectra; EPR spectra; repeating and stability photocatalytic results; band gap analysis; EIS Nyquist plots (PDF)

■ AUTHOR INFORMATION

Corresponding Authors

*E-mail: sunzy@mail.buct.edu.cn (Z.S.).
*E-mail: jianggy@cup.edu.cn (G.J.).
*E-mail: wangbaojun@tyut.edu.cn (B.W.).

ORCID

Shaobin Wang: 0000-0002-1751-9162
Zhenyu Sun: 0000-0001-5788-9339

Author Contributions

The paper was written by S.L. and revised by S.W. and Z.S. DFT calculations were performed by B.W. through contributions of all authors. S.H. did TEM measurements. T.W. and Y.S. performed XANES measurements. The project was supervised by Z.S.

Notes

The authors declare no competing financial interest.

■ ACKNOWLEDGMENTS

This work was supported by the State Key Laboratory of Organic−Inorganic Composites (No. oic-201503005); the Beijing Natural Science Foundation (2192039); the Beijing National Laboratory for Molecular Sciences (BNLMS2016-0133); the State Key Laboratory of Separation Membranes and Membrane Processes (Tianjin Polytechnic University, No. M2-201704); Key Project of the National Natural Science Foundation of China (No. 21736007).

■ REFERENCES

(1) Shi, M.-M.; Bao, D.; Wulan, B.-R.; Li, Y.-H.; Zhang, Y.-F.; Yan, J.-M.; Jiang, Q. Au Sub-Nanoclusters on TiO_2 toward Highly Efficient and Selective Electrocatalyst for N_2 Conversion to NH_3 at Ambient Conditions. *Adv. Mater.* **2017**, *29* (17), 1606550.

(2) Rajan Premkumar, J.; Ramaraj, R. Photochemical Reduction of Nitrite to Ammonia at A Solid Phase Photoredox System. *Chem. Commun.* **1998**, *11*, 1195−1196.

(3) Schrauzer, G. N.; Guth, T. D. Photocatalytic reactions: Photolysis of Water and Photoreduction of Nitrogen on Titanium Dioxide. *J. Am. Chem. Soc.* **1977**, *99* (22), 7189−7193.

(4) Malato, S.; Blanco, J.; Vidal, A.; Richter, C. Photocatalysis with Solar Energy at A Pilot-plant Scale: An Overview. *Appl. Catal., B* **2002**, *37* (1), 1−15.

(5) Li, C.; Wang, T.; Zhao, Z.; Yang, W.; Li, J.; Li, A.; Yang, Z.; Ozin, G. A.; Gong, J. Promoted Fixation of Molecular Nitrogen with Surface Oxygen Vacancies on Plasmon-Enhanced TiO_2 Photoelectrodes. *Angew. Chem., Int. Ed.* **2018**, *57* (19), 5278−5282.

(6) Sun, S.; Li, X.; Wang, W.; Zhang, L.; Sun, X. Photocatalytic Robust Solar Energy Reduction of Dinitrogen to Ammonia on Ultrathin MoS_2. *Appl. Catal., B* **2017**, *200*, 323−329.

(7) Chen, X.; Li, N.; Kong, Z.; Ong, W.; Zhao, X. Photocatalytic Fixation of Nitrogen to Ammonia: State-of-the-art Advancements and Future Prospects. *Mater. Horiz.* **2018**, *5* (1), 9−27.

(8) Dong, G.; Ho, W.; Wang, C. Selective Photocatalytic N_2 Fixation Dependent on g-C_3N_4 Induced by Nitrogen Vacancies. *J. Mater. Chem. A* **2015**, *3* (46), 23435−23441.

(9) Ma, H.; Shi, Z.; Li, S.; Liu, N. Large-scale Production of Graphitic Carbon Nitride with Outstanding Nitrogen Photofixation Ability via A Convenient Microwave Treatment. *Appl. Surf. Sci.* **2016**, *379*, 309−315.

(10) Chen, S.; Perathoner, S.; Ampelli, C.; Mebrahtu, C.; Su, D.; Centi, G. Electrocatalytic Synthesis of Ammonia at Room Temperature and Atmospheric Pressure from Water and Nitrogen on a Carbon-Nanotube-Based Electrocatalyst. *Angew. Chem.* **2017**, *129* (10), 2743−2747.

(11) Qiu, P.; Xu, C.; Zhou, N.; Chen, H.; Jiang, F. Metal-Free Black Phosphorus Nanosheets-Decorated Graphitic Carbon Nitride Nanosheets with CP Bonds for Excellent Photocatalytic Nitrogen Fixation. *Appl. Catal., B* **2018**, *221*, 27−35.

(12) Li, H.; Shang, J.; Ai, Z.; Zhang, L. Efficient Visible Light Nitrogen Fixation with BiOBr Nanosheets of Oxygen Vacancies on the Exposed {001} Facets. *J. Am. Chem. Soc.* **2015**, *137* (19), 6393−6399.

(13) Janet, C. M.; Navaladian, S.; Viswanathan, B.; Varadarajan, T. K.; Viswanath, R. P. Heterogeneous Wet Chemical Synthesis of Superlattice-Type Hierarchical ZnO Architectures for Concurrent H_2 Production and N_2 Reduction. *J. Phys. Chem. C* **2010**, *114* (6), 2622−2632.

(14) Sheng, Y.; Yang, J.; Wang, F.; Liu, L.; Liu, H.; Yan, C.; Guo, Z. Sol-Gel Synthesized Hexagonal Boron Nitride/Titania Nanocomposites with Enhanced Photocatalytic Activity. *Appl. Surf. Sci.* **2019**, *465*, 154−163.

(15) Low, J.; Cheng, B.; Yu, J. Surface Modification and Enhanced Photocatalytic CO_2 Reduction Performance of TiO_2: A Review. *Appl. Surf. Sci.* **2017**, *392*, 658−686.

DOI: 10.1021/acssuschemeng.8b06134
ACS Sustainable Chem. Eng. 2019, 7, 6813−6820

(16) Uyguner-Demirel, C. S.; Birben, N. C.; Bekbolet, M. Elucidation of Background Organic Matter Matrix Effect on Photocatalytic Treatment of Contaminants Using TiO_2: A Review. *Catal. Today* **2017**, *284*, 202−214.
(17) Laxma Reddy, P. V.; Kavitha, B.; Kumar Reddy, P. A.; Kim, K.-H. TiO_2-Based Photocatalytic Disinfection of Microbes in Aqueous Media: A Review. *Environ. Res.* **2017**, *154*, 296−303.
(18) Hoshino, K. New Avenues in Dinitrogen Fixation Research. *Chem. - Eur. J.* **2001**, *7* (13), 2727−2731.
(19) Comer, B. M.; Medford, A. J. Analysis of Photocatalytic Nitrogen Fixation on Rutile TiO_2(110). *ACS Sustainable Chem. Eng.* **2018**, *6* (4), 4648−4660.
(20) Linsebigler, A. L.; Lu, G.; Yates, J. T. Photocatalysis on TiO_2 Surfaces: Principles, Mechanisms, and Selected Results. *Chem. Rev.* **1995**, *95* (3), 735−758.
(21) Pandikumar, A.; Manonmani, S.; Ramaraj, R. TiO_2-Au Nanocomposite Materials Embedded in Polymer Matrices and Their Application in The Photocatalytic Reduction of Nitrite to Ammonia. *Catal. Sci. Technol.* **2012**, *2* (2), 345−353.
(22) Ogawa, T.; Kitamura, T.; Shibuya, T.; Hoshino, K. Characterization and Material Conditions of Conducting Polymer/Titanium Oxide Hybrid Systems Used for Dinitrogen Fixation Under Ordinary Pressure and Temperature. *Electrochem. Commun.* **2004**, *6* (1), 55−60.
(23) Ranjit, K. T.; Varadarajan, T. K.; Viswanathan, B. Photocatalytic Reduction of Dinitrogen to Ammonia over Noble-metal-loaded TiO_2. *J. Photochem. Photobiol., A* **1996**, *96* (1), 181−185.
(24) Sun, Z. Y.; Talreja, N.; Tao, H.; Texter, J.; Muhler, M.; Strunk, J.; Chen, J. Catalysis of Carbon Dioxide Photoreduction on Nanosheets: Fundamentals and Challenges. *Angew. Chem., Int. Ed.* **2018**, *57* (26), 7610−7627.
(25) Zhao, W.; Zhang, J.; Zhu, X.; Zhang, M.; Tang, J.; Tan, M.; Wang, Y. Enhanced Nitrogen Photofixation on Fe-doped TiO_2 with Highly Exposed (101) Facets in The Presence of Ethanol as Scavenger. *Appl. Catal., B* **2014**, *144*, 468−477.
(26) Linnik, O. P.; Kisch, H. Dinitrogen Photofixation at Ruthenium-modified Titania Films. *Mendeleev Commun.* **2008**, *18* (1), 10−11.
(27) Peng, P.; Cheng, Y.; Hatzenbeller, R.; Addy, M.; Zhou, N.; Schiappacasse, C.; Chen, D.; Zhang, Y.; Anderson, E.; Liu, Y.; Chen, P.; Ruan, R. Ru-Based Multifunctional Mesoporous Catalyst for Low-Pressure and Non-thermal Plasma Synthesis of Ammonia. *Int. J. Hydrogen Energy* **2017**, *42* (30), 19056−19066.
(28) Honkala, K.; Hellman, A.; Remediakis, I. N.; Logadottir, A.; Carlsson, A.; Dahl, S.; Christensen, C. H.; Noerskov, J. K. Ammonia Synthesis From First-Principles Calculations. *Science* **2005**, *307* (5709), 555.
(29) Li, L.; Wang, Y.; Vanka, S.; Mu, X.; Mi, Z.; Li, C.-J. Nitrogen Photofixation over III-Nitride Nanowires Assisted by Ruthenium Clusters of Low Atomicity. *Angew. Chem., Int. Ed.* **2017**, *56* (30), 8701−8705.
(30) Tao, H.; Choi, C.; Ding, L.-X.; Jiang, Z.; Han, Z.; Jia, M.; Fan, Q.; Gao, Y.; Wang, H.; Robertson, A. W.; Hong, S.; Jung, Y.; Liu, S.; Sun, Z. Y. Nitrogen Fixation by Ru Single-Atom Electrocatalytic Reduction. *Chem.* **2019**, *5*, 204−214.
(31) Zhu, C.; Fu, S.; Shi, Q.; Du, D.; Lin, Y. Single-Atom Electrocatalysts. *Angew. Chem., Int. Ed.* **2017**, *56* (45), 13944−13960.
(32) Gao, G.; Jiao, Y.; Waclawik, E. R.; Du, A. Single Atom (Pd/Pt) Supported on Graphitic Carbon Nitride as an Efficient Photocatalyst for Visible-Light Reduction of Carbon Dioxide. *J. Am. Chem. Soc.* **2016**, *138* (19), 6292−6297.
(33) Wang, Y.; Zhao, X.; Cao, D.; Wang, Y.; Zhu, Y. Peroxymonosulfate Enhanced Visible Light Photocatalytic Degradation Bisphenol A by Single-Atom Dispersed Ag Mesoporous g-C_3N_4 Hybrid. *Appl. Catal., B* **2017**, *211*, 79−88.
(34) Trofimovaite, R.; Parlett, C. M. A.; Kumar, S.; Frattini, L.; Isaacs, M. A.; Wilson, K.; Olivi, L.; Coulson, B.; Debgupta, J.; Douthwaite, R. E.; Lee, A. F. Single Atom Cu(I) Promoted Mesoporous Titanias for Photocatalytic Methyl Orange Depollution and H_2 Production. *Appl. Catal., B* **2018**, *232*, 501−511.
(35) Antoniadou, M.; Vaiano, V.; Sannino, D.; Lianos, P. Photocatalytic Oxidation of Ethanol Using Undoped and Ru-Doped titania: Acetaldehyde, Hydrogen or Electricity Generation. *Chem. Eng. J.* **2013**, *224*, 144−148.
(36) Yang, H. G.; Sun, C. H.; Qiao, S. Z.; Zou, J.; Liu, G.; Smith, S. C.; Cheng, H. M.; Lu, G. Q. Anatase TiO_2 Single Crystals with A Large Percentage of Reactive Facets. *Nature* **2008**, *453* (7195), 638−641.
(37) Shen, J. Y.; Adnot, A.; Kaliaguine, S. An ESCA Study of the Interaction of Oxygen with the Surface of Ruthenium. *Appl. Surf. Sci.* **1991**, *51* (1), 47−60.
(38) Lei, F.; Sun, Y.; Liu, K.; Gao, S.; Liang, L.; Pan, B.; Xie, Y. Oxygen Vacancies Confined in Ultrathin Indium Oxide Porous Sheets for Promoted Visible-Light Water Splitting. *J. Am. Chem. Soc.* **2014**, *136* (19), 6826−6829.
(39) Ingemar Odenbrand, C. U.; Anderson, S. L. T. Hydrogenation of Benzene to Cyclohexene on An Unsupported Ruthenium Catalyst: An Esca Study of Titanium Poisoned Catalysts. *J. Chem. Technol. Biotechnol., Chem. Technol.* **1983**, *33* (3), 150−156.
(40) Jiang, Z.; Ding, D.; Wang, L.; Zhang, Y.; Zan, L. Interfacial Effects of MnO_x-loaded TiO_2 with Exposed {001} Facets and Its Catalytic Activity for The Photoreduction of CO_2. *Catal. Sci. Technol.* **2017**, *7* (14), 3065−3072.
(41) Liu, P.; Zhao, Y.; Qin, R.; Mo, S.; Chen, G.; Gu, L.; Chevrier, D. M.; Zhang, P.; Guo, Q.; Zang, D.; Wu, B.; Fu, G.; Zheng, N. Photochemical Route for Synthesizing Atomically Dispersed Palladium Catalysts. *Science* **2016**, *352* (6287), 797−800.
(42) Wang, X.; Chen, W.; Zhang, L.; Yao, T.; Liu, W.; Lin, Y.; Ju, H.; Dong, J.; Zheng, L.; Yan, W.; Zheng, X.; Li, Z.; Wang, X.; Yang, J.; He, D.; Wang, Y.; Deng, Z.; Wu, Y.; Li, Y. Uncoordinated Amine Groups of Metal−Organic Frameworks to Anchor Single Ru Sites as Chemoselective Catalysts toward the Hydrogenation of Quinoline. *J. Am. Chem. Soc.* **2017**, *139* (28), 9419−9422.
(43) Manole, A. V.; Dobromir, M.; Apetrei, R.; Nica, V.; Luca, D. Surface Characterization of Sputtered N:TiO_2 Thin Films within a Wide Range of Dopant Concentration. *Ceram. Int.* **2014**, *40* (7), 9989−9995.
(44) Khan, M. M.; Ansari, S. A.; Pradhan, D.; Ansari, M. O.; Han, D. H.; Lee, J.; Cho, M. H. Band Gap Engineered TiO_2 Nanoparticles for Visible Light Induced Photoelectrochemical and Photocatalytic Studies. *J. Mater. Chem. A* **2014**, *2* (3), 637−644.
(45) Scanlon, D. O.; Dunnill, C. W.; Buckeridge, J.; Shevlin, S. A.; Logsdail, A. J.; Woodley, S. M.; Catlow, C. R. A.; Powell, M. J.; Palgrave, R. G.; Parkin, I. P.; Watson, G. W.; Keal, T. W.; Sherwood, P.; Walsh, A.; Sokol, A. A. Band Alignment of Rutile and Anatase TiO_2. *Nat. Mater.* **2013**, *12*, 798.
(46) Bikondoa, O.; Pang, C. L.; Ithnin, R.; Muryn, C. A.; Onishi, H.; Thornton, G. Direct Visualization of Defect-mediated Dissociation of Water on TiO_2(110). *Nat. Mater.* **2006**, *5*, 189.
(47) Wan, J.; Chen, W.; Jia, C.; Zheng, L.; Dong, J.; Zheng, X.; Wang, Y.; Yan, W.; Chen, C.; Peng, Q.; Wang, D.; Li, Y. Defect Effects on TiO_2 Nanosheets: Stabilizing Single Atomic Site Au and Promoting Catalytic Properties. *Adv. Mater.* **2018**, *30* (11), 1705369.
(48) Yi, S.; Yan, J.; Wulan, B.; Li, S.; Liu, K.; Jiang, Q. Noble-metal-free Cobalt Phosphide Modified Carbon Nitride: An Efficient Photocatalyst for Hydrogen Generation. *Appl. Catal., B* **2017**, *200*, 477−483.
(49) Hirakawa, H.; Hashimoto, M.; Shiraishi, Y.; Hirai, T. Photocatalytic Conversion of Nitrogen to Ammonia with Water on Surface Oxygen Vacancies of Titanium Dioxide. *J. Am. Chem. Soc.* **2017**, *139* (31), 10929−10936.
(50) Zhao, J.; Zhao, J.; Cai, Q. Single Transition Metal Atom Embedded into A MoS_2 Nanosheet as A Promising Catalyst for Electrochemical Ammonia Synthesis. *Phys. Chem. Chem. Phys.* **2018**, *20* (14), 9248−9255.
(51) Wang, B.; Cai, H.; Shen, S. Single Metal Atom Photocatalysis. *Small Methods* **2019**, 1800447.

DOI: 10.1021/acssuschemeng.8b06134
ACS Sustainable Chem. Eng. 2019, 7, 6813−6820

(52) Jia, M.; Fan, Q.; Liu, S.; Qiu, J.; Sun, Z. Single-Atom Catalysis for Electrochemical CO_2 Reduction. *Curr. Opini. Green Sustainable Chem.* **2019**, *16*, 1−6.

DOI: 10.1021/acssuschemeng.8b06134
ACS Sustainable Chem. Eng. 2019, 7, 6813−6820